

Optically induced orientational transitions in nematic liquid crystals with planar alignment

Dmitry O. Krimer

Max Planck Institute for the Physics of Complex Systems, Nöthnitzer Strasse 38, D-01187 Dresden, Germany

(Received 1 October 2008; published 26 March 2009)

A theoretical study of dynamical phenomena induced by linearly polarized light incident perpendicularly on a planar aligned nematic layer with the light intensity as the control parameter is reported. We find the threshold of the optically induced twist Fréedericksz transition as a function of the problem parameters. The critical light intensity was found substantially lower than predicted earlier by Santamato *et al.* [Phys. Rev. A **36**, 2389 (1987)]. We have demonstrated by a rigorous stability analysis that the bifurcation is stationary only for a thickness of the nematic layer smaller than a certain critical value and becomes a Hopf bifurcation in the opposite case. Above the Hopf bifurcation an oscillatory state appears. It becomes unstable at a secondary threshold through a heteroclinic bifurcation, and the director settles to a new stationary distorted state.

DOI: [10.1103/PhysRevE.79.030702](https://doi.org/10.1103/PhysRevE.79.030702)

PACS number(s): 42.70.Df, 05.45.-a, 42.65.Sf

The optical phenomena exhibited by nematic liquid crystals have been a subject of intensive study during the last few decades. Nematics are optically anisotropic uniaxial materials; their local optical properties are determined by the orientation of the director $\mathbf{n}(\mathbf{r}, t)$. The dielectric tensor governing the propagation of light is anisotropic and depends on \mathbf{n} . There are two competing mechanisms that determine the alignment in the bulk of the nematic. On one hand, it is enforced by the director orientation at the confining substrates. On the other hand, the electric field of the incident light exerts a torque on the director which may conflict with the boundary-imposed alignment. The torque increases with an increase in the light intensity. Eventually, at a certain light intensity, the boundary-imposed alignment becomes unstable and is replaced by the light-imposed one (optically induced Fréedericksz transition), which in turn affects light propagation [1]. A large variety of nonlinear phenomena occurs as a result of this feedback [2]. For instance, the precession of the molecules after director reorientation has a clear interpretation, as being due to angular momentum transfer from the light to the medium (the so-called self-induced stimulated light scattering [3]). During this process some of the photons are scattered, reversing their helicity, and the change in their angular momentum is transferred to the nematic. The scattered photons acquire a slight redshift, transmitting the energy to the rotating molecules. The possibility of dynamical changes of the refractive index in a nematic employing the orientational phenomena has attracted much attention recently in the context of all-optical devices based on photonic structures infiltrated with liquid crystals (see, e.g., [4]).

The goal of this paper is a detailed theoretical study of light-induced phenomena in a nematic cell with planar alignment (the director is oriented parallel to the confining planes). Compared to the case of homeotropic geometry (the director is oriented perpendicular to the confining planes), the planar geometry is much less explored. To our knowledge, this problem was considered before in [5] where adiabatic light propagation (the polarization of light follows the direction of \mathbf{n}) and a simple one-mode approximation for the director deformation were assumed. A more complicated situation with nonadiabatic light propagation and arbitrary phase delay was explored in [6] with the assumption that the planar state loses its stability via homogeneous stationary

bifurcation. In a recent paper [7], a linear stability analysis with respect to spatially stationary periodic perturbations in the plane of the layer was performed in the limit of very thin layers. From this paper one concludes that the primary bifurcation is spatially periodic for $K_2/K_1 > 3.3$ while for common nematics $K_2/K_1 < 1$. (Here K_2 and K_1 are, respectively, the twist and splay elastic constants.) The thresholds for stationary homogeneous bifurcation found in [6] turned out to be rather high with a very twisted director profile at the onset. The question arises: Could it be that in a certain range of parameters a Hopf bifurcation occurs prior to the stationary bifurcation? Here we perform a general stability analysis with respect to arbitrary homogeneous perturbations. The great difference between the actual ratio of the elastic constants and the one corresponding to a primary spatially periodic bifurcation for a thin layer [7] provides grounds to expect the spatial homogeneity of the primary bifurcation in the entire region inspected in the present paper, i.e., at least unless the thickness of the layer becomes a large quantity. We find that the primary threshold is stationary when the thickness of the layer is smaller than a certain critical value, which is in accordance with previous studies. However, above this value the threshold for the homogeneous Hopf bifurcation is substantially lower than the thresholds found for the stationary homogeneous [6] and spatially periodic instabilities [7]. In contrast to the previous studies, we present a detailed numerical analysis in the nonlinear regime well above the threshold for arbitrary values of the phase delay and nonadiabatic propagation of light. We assume that the transverse cross section of the beam is much larger than the thickness of the cell (the so-called plane wave approximation), and the spatial dependence of all physical quantities is restricted to the coordinate perpendicular to the layer.

We consider a plane wave linearly polarized along the y direction, propagating along the z axis. The wave is incident perpendicularly on a nematic layer (see Fig. 1). Initially the director is orientated along the x axis (planar alignment) and keeps its orientation at the boundaries (rigid boundary conditions). To describe the director orientation the twist angle $\Phi(z, t)$ is introduced, so that $\mathbf{n} = (\cos \Phi, \sin \Phi, 0)$. The starting point is the set of nematodynamic equations coupled with Maxwell's equations for the propagation of light [8]. The dynamical equation of motion for $\Phi(z, t)$ is obtained from

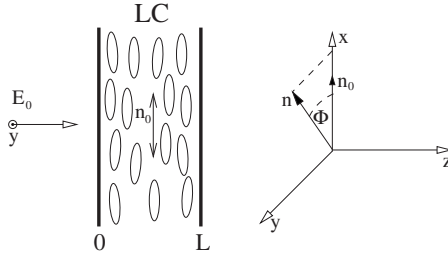


FIG. 1. Geometry of the setup: linearly polarized light along the y direction incident perpendicularly on a nematic layer with the director $\mathbf{n}_0 \parallel \mathbf{x}$ (planar state). The components of the director \mathbf{n} are described in terms of the twist angle Φ .

the balance of torques (elastic, electromagnetic, and viscous) acting on the director. The components of the electric field might be represented in terms of the ordinary (o) and extraordinary (e) amplitudes of the waves A_e, A_o which vary slowly with z on the scale $(k_0 L)^{-1}$ (see, e.g., [9]), where $k_0 = \omega/c$ is the wave number of the incident wave and L stands for the layer thickness. Finally, the coupled partial differential equation PDE for Φ and ordinary differential equations (ODEs) for A_e and A_o (no velocity field) can be written as [9]

$$\partial_t \Phi = \partial_z^2 \Phi + 2\rho \tilde{k}_0^2 \operatorname{Re}(A_e A_o^* e^{ik_0 z}), \quad (1)$$

$$\partial_z A_o = -(\partial_z \Phi) e^{ik_0 z} A_e, \quad \partial_z A_e = (\partial_z \Phi) e^{-ik_0 z} A_o, \quad (2)$$

where $\tilde{k}_0 = 2L\delta n/\lambda$ is the dimensionless thickness (proportional to the phase delay) with $\delta n = n_e - n_o$ (n_e and n_o are the refractive indices of the ordinary and extraordinary light, respectively) and λ is the incident light wavelength. To make the variables in Eqs. (1) and (2) dimensionless they have undergone the scale transformation $t \rightarrow t/\tau$, $z \rightarrow \pi z/L$; the amplitudes $A_{e,o}$ have been normalized over the electric field amplitude of the incident light; and $\rho = I/I_c$, where I stands for the incident light intensity. Here $\tau = \gamma_1 L^2 / \pi^2 K_2$ is the characteristic relaxation time of the director motion, $I_c = 8\pi^2 c K_2 n_e \delta n / \lambda^2 (n_e + n_o)$, and $\gamma_1 = \alpha_3 - \alpha_2$ is the rotational viscosity.

The boundary condition for Φ and initial conditions for A_o and A_e at $z=0$ read

$$\Phi_{z=0, \pi}(t) = 0, \quad |A_{o0}|^2 = 1, \quad |A_{e0}|^2 = 0, \quad A_{e0} A_{o0}^* = 0. \quad (3)$$

Note that, owing to the reflection symmetry with respect to the y direction, Eqs. (1)–(3) are invariant under the transformation $S: \{\Phi, A_e, A_o\} \rightarrow \{-\Phi, \mp A_e, \pm A_o\}$. It is convenient to represent the solution of Eqs. (1)–(3) as a series $\Phi(z, t) = \sum_n \phi_n(t) \sin(nz)$, where each term of the sum satisfies the boundary conditions Eq. (3) identically. Then, Eqs. (1)–(3) are transformed into an infinite set of coupled equations for ϕ_n . To make the problem tractable, the expansion for Φ is truncated at a certain large enough number of equations, N , which are solved numerically by the standard Runge-Kutta method. The error caused by the truncation is controlled by test runs with double and triple the number of modes. For every set of parameters, N is selected so that the difference between the routine and test runs is better than 1%. The results below are obtained for $N=20$, which is within this

accuracy. In addition, we perform numerically a linear stability analysis of the stationary distorted states ($\partial_t \phi_n = 0$).

The starting point of the study is the linear stability analysis of the planar state $\Phi(z, t) = 0$. The linearized integro-differential equation for $\Phi(z, t) = \Phi(z) \exp(\sigma t)$ is as follows:

$$\partial_z^2 \Phi + 2\rho \tilde{k}_0^2 \left(\Phi + \tilde{k}_0 \int_0^z \Phi(z') \sin[\tilde{k}_0(z' - z)] dz' \right) = \sigma \Phi. \quad (4)$$

It results in the following set of equations for ϕ_n (eigenvalue problem):

$$\sum_n A_{mn} \phi_n = \sigma \phi_m, \quad A_{mn} = \left(\frac{2\rho \tilde{k}_0^2}{n^2 - \tilde{k}_0^2} - 1 \right) n^2 \delta_{mn} + \frac{4(-1)^m \rho \tilde{k}_0^3 m n \sin(\pi \tilde{k}_0)}{\pi(m^2 - \tilde{k}_0^2)(n^2 - \tilde{k}_0^2)}. \quad (5)$$

The solvability condition for Eq. (5) requires $\det(A - \sigma I) = 0$. It brings about an infinite number of eigenvalues σ_n . However, at $n \gg \tilde{k}_0$ or (and) $m \gg \tilde{k}_0$ the off-diagonal elements of matrix A_{mn} decay as $1/n$ or (and) $1/m$, while the diagonal elements are approximately $-n^2$. Then, in the leading approximation $\det(A - \sigma I)$ factorizes for a product of an infinite number of the diagonal elements at $n > N$ (which gives stable real eigenvalues $\sigma_n \approx -n^2$ related to elastic relaxation) and a matrix $N \times N$, where $N \gg \tilde{k}_0$. The eigenvalues of the matrix are related to light-induced perturbations and should be inspected more carefully. These arguments provides us with the natural truncation scale $\sim \tilde{k}_0$. The planar state loses stability when the real part of (at least) one of the eigenvalues, $\operatorname{Re}(\sigma_n)$, becomes positive. It should be stressed that the matrix A_{mn} is not Hermitian and may have complex eigenvalues; in other words, unstable modes may be oscillatory.

Typical results of the discussed stability analysis are presented in Fig. 2, where $\operatorname{Re}(\sigma_n)$ and $\operatorname{Im}(\sigma_n)$ versus ρ are shown for $\tilde{k}_0 = 1.6$. It is seen that $\operatorname{Re}(\sigma_n)$ forms a tongued structure with a family of branches which, at first, appear as pairs of purely real branches that go almost parallel to each other as ρ increases, but then the pair merges at a certain $\rho \geq \rho_{\text{top}}^{(n)}$. Next, the branches continue as a pair of complex conjugate modes. Some of the purely real branches cross the zero line at intensities ρ given by the formula

$$\frac{2\rho \sin(\pi \tilde{k}_0 \sqrt{1 + 2\rho})}{\pi \tilde{k}_0 \sqrt{1 + 2\rho}} = -1, \quad (6)$$

which was derived in [6]. The first two tongues depicted by shaded areas cross the abscissa at $\rho_1^* = 16.6$, $\rho_2^* = 17.8$, $\rho_3^* = 24.3$, and $\rho_4^* = 26.5$, respectively, and are the same as those shown in Fig. 1 of [6]. (The dimensionless $\tilde{L} = 5$ introduced there corresponds to $\tilde{k}_0 = \tilde{L}/\pi \sim 1.6$ used in our calculations.) In [6] this structure was interpreted as a series of alternating stable and unstable intervals for the planar state as the light intensity increases, with the lowest threshold for instability

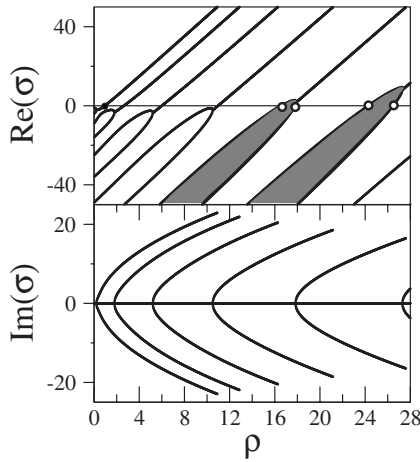


FIG. 2. $\text{Re}(\sigma)$ and $\text{Im}(\sigma)$ vs ρ for $\tilde{k}_0=1.6$. Filled circle: primary threshold ($\rho_1=0.95$, Hopf bifurcation). Shaded tongues cross abscissa at, respectively, $\rho_1^*=16.6$, $\rho_2^*=17.8$, $\rho_3^*=24.3$, and $\rho_4^*=26.5$, depicted by empty circles.

given by $\rho_1^*=16.6$. However, in reality, the planar state loses stability via a Hopf bifurcation at a much lower value $\rho_1=0.95$ (filled circle in Fig. 2) and never regains stability at higher intensities again. In fact, the reason for this difference from the results of [6] is that only a stationary bifurcation was considered. As a result, the growth rate was *a priori* real instead of being complex and, thus the growth rates with $\text{Im}(\sigma) \neq 0$ predicted here were not caught. The stability diagram in the (\tilde{k}_0, ρ) plane is shown in Fig. 3 by solid lines and the thresholds calculated using Eq. (6) are depicted by dashed lines. It is interesting that, below a critical value $\tilde{k}_0^{(c)}=0.64$ (corresponding to $\tilde{L}=2$ in [6]), the primary bifurcation is indeed stationary and the values of thresholds are correctly described by Eq. (6). In that case, the very first tongue crosses the ρ axis (in contrast to the situation for $\tilde{k}_0=1.6 > \tilde{k}_0^{(c)}$ depicted in Fig. 2, where the first tongue is under the abscissa) and at the threshold the largest growth rate corresponds to the purely real branch. When $\tilde{k}_0^{(c)}$ is approached from below, this first tongue goes down and, finally, at $\tilde{k}_0=\tilde{k}_0^{(c)}$ the whole tongue lies under the ρ axis. Note

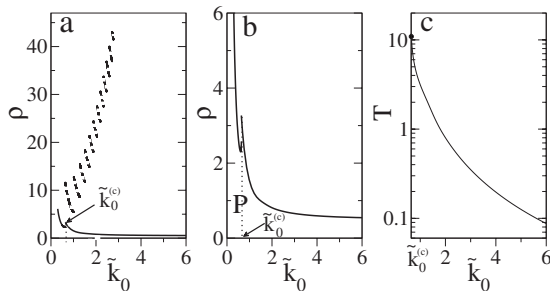


FIG. 3. (a),(b) Solid lines: stability diagram of the planar state on the (\tilde{k}_0, ρ) plane. Dashed lines on (a): thresholds calculated using Eq. (6). Solid line with $\tilde{k}_0 < \tilde{k}_0^{(c)}$ ($\tilde{k}_0 \geq \tilde{k}_0^{(c)}$) corresponds to stationary (Hopf) bifurcation. P is the region of stability of the planar state. (c) Period of oscillation of Φ at the onset for $\tilde{k}_0 \geq \tilde{k}_0^{(c)}$ (Hopf bifurcation).

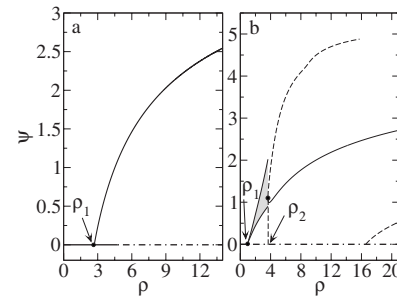


FIG. 4. Bifurcation diagrams for (a) $\tilde{k}_0=0.5$ and (b) $\tilde{k}_0=1.6$: parameter of reorientation Ψ vs ρ . Solid (dashed) curves correspond to stable (unstable) stationary solutions. ρ_1 is the primary instability of the planar state. (a) $\rho_1=2.7$ (stationary bifurcation) and (b) $\rho_1=0.95$ (Hopf bifurcation). Gray region (confined by two lines) shows the oscillatory states of the director. $\rho_2=3.65$ is the secondary instability (heteroclinic bifurcation).

that transition to another branch with $\text{Im}(\sigma) \neq 0$ is accompanied by a stepwise change of the threshold intensity. Such behavior is related to the inclined structure of the tongues (see Fig. 3). It should be stressed that, for $\tilde{k}_0 > \tilde{k}_0^{(c)}$, the true values of the thresholds differ from the ones predicted by Eq. (6) by one order, and with increase of \tilde{k}_0 quite rapidly, by two orders of magnitude. The true threshold of the Hopf primary instability decreases with an increase in \tilde{k}_0 from $I=3.3I_c$ at $\tilde{k}_0=\tilde{k}_0^{(c)}$ to $0.5I_c$ at $\tilde{k}_0=8$, and then practically does not change for further increase in the \tilde{k}_0 (see Fig. 3). Interestingly, the period of oscillation of the twist angle at the onset of Hopf bifurcation decreases by two orders of magnitude within an interval $\tilde{k}_0 \in [\tilde{k}_0^{(c)}, 6]$ [see Fig. 3(c)]. To obtain a stability diagram in the dimensional (L, I) plane one should rescale the \tilde{k}_0 and ρ axes of Fig. 3, multiplying them by $\lambda/(2\delta n)$ and I_c , respectively. To avoid very large values for thresholds in experiment, one should take nematics with rather small values of δn . For instance, for $\delta n=5 \times 10^{-3}$, $K_2=2.5 \times 10^{-7}$ dyn, and $\lambda=532$ nm, the value of I_c is 52 kW/cm^2 and the critical length $L^{(c)}=\tilde{k}_0^{(c)}\lambda/(2\delta n)$ is $34 \mu\text{m}$.

It is worth noting that the linear integrodifferential equation (5) appears in the framework of linear analysis of another problem, namely, that with a linearly polarized ordinary light wave incident at a small oblique angle on a thin layer of homeotropically oriented nematic [10,11]. The only difference is that there one deals with the incidence angle κ instead of \tilde{k}_0 used here. The stability diagram in the (ρ, κ) plane consists of a line of stationary instability for $\kappa < \kappa^{(c)}$ and a line of Hopf bifurcations in the opposite case. The stationary instability is indeed described by the formula (6) after it is rewritten in corresponding quantities. Above $\kappa^{(c)}$ the homeotropic state loses stability via a Hopf bifurcation and the formula (6) is no longer applicable.

We choose a sum of squares of all modes $\Psi=\sum_n \phi_n^2$ as a theoretical measure of reorientation inside a nematic. In Fig. 4 typical bifurcation diagrams are shown. The planar state remains stable when $\rho < \rho_1$. At $\rho=\rho_1$ we deal with a continuous transition via either a stationary bifurcation for $\tilde{k}_0 < \tilde{k}_0^{(c)}$

or a Hopf bifurcation in the opposite case. Above the threshold and for $\tilde{k}_0 < \tilde{k}_0^{(c)}$, the director settles to a stationary distorted state, whereas for $\tilde{k}_0 > \tilde{k}_0^{(c)}$ it settles to an oscillatory one. In the latter regime, the lower and upper lines depicted in Fig. 4(b) bound the region in gray and correspond to the minimum and maximum values taken by Ψ during its oscillation. The director motion develops along the limit cycle in the space of ϕ_n (which is infinite). In some narrow region around $\rho_2=3.65$, the period of oscillations increases progressively with increasing light intensity, and oscillations become substantially anharmonic. The period diverges at $\rho=\rho_2$ which corresponds to a secondary bifurcation into a new stationary distorted state. The dynamics near the threshold is summarized in the projection of the true phase trajectory on the plane (ϕ_1, ϕ_2) (see Fig. 5). The bifurcation at $\rho=\rho_2$ belongs to a rather rare type and corresponds to the following. Above ρ_2 a system has two pairs of stationary nontrivial solutions which are mutual images under the symmetry transformation S . The first pair is represented by a stable node and its image, and the second one by a saddle and its image. There is also a trivial solution which is represented by an unstable focus corresponding to the spatially uniform planar state. Starting from different initial conditions the system eventually settles to one of the stable nodes. A separatrix, which divides the phase plane into the basins of attraction for the two stable nodes, goes through the two saddles and the unstable focus. As ρ_2 is approached from above, the saddle and node go closer and closer to each other and finally merge at $\rho=\rho_2$. At this point a limit cycle appears, which exists for $\rho_1 < \rho < \rho_2$. It is worth noting that the symmetry S is spontaneously broken at the secondary bifurcation.

In conclusion, we have studied theoretically the transitions induced by linearly polarized light incident perpendicularly onto a layer of nematic that has initial planar alignment. We have found the primary threshold as a function of thickness of the layer by performing a linear stability analysis of the basic state. It has been found that with increasing light intensity the planar state becomes unstable in favor of either a stationary distorted state when the thickness is below a certain critical value, or an oscillatory state if the thickness is

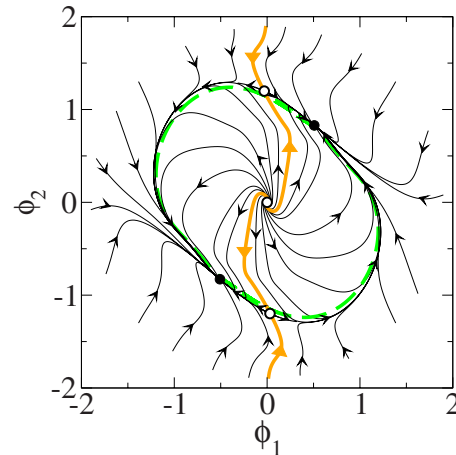


FIG. 5. (Color online) Dynamics near the secondary threshold $\rho_2=3.6530$. Thin black lines: director trajectories at $\rho=3.7967 > \rho_2$ in the plane of the first two modes (ϕ_1, ϕ_2) . Starting from different initial conditions, the system settles to one of the two stable nodes (filled circles). Orange (thick gray) curve: separatrix. Empty circles: unstable fixed points (saddles). Origin: unstable spatially uniform planar state (focus). Green (gray) dashed line: limit cycle at $\rho=3.638 < \rho_2$.

above critical. As the intensity increases further, the oscillatory state disappears via a secondary bifurcation. At the bifurcation point two identical saddle-node fixed points are created on opposite sites of the limit cycle. This results in divergence of the period of oscillations and separation of the limit cycle into two heteroclinic orbits. Further increase of the intensity brings about splitting of each fixed point into a stable node and a saddle. In typical cases the calculated thresholds have values substantially lower than those believed before. Competition between homogeneous and spatially periodic instabilities for thick layers ($\tilde{k}_0 \gg 1$) might be a subject of future study.

The author wishes to thank M. I. Tribelsky, S. Flach, A. Miroshnichenko, E. Brasselet, and A. Krekhov for helpful discussions and comments.

-
- [1] N. V. Tabiryan, A. V. Sukhov, and B. Y. Zel'dovich, *Mol. Cryst. Liq. Cryst.* **136**, 1 (1986).
 - [2] G. Demeter and D. O. Krimer, *Phys. Rep.* **448**, 133 (2007).
 - [3] E. Santamato, M. Romagnoli, M. Settembre, B. Daino, and Y. R. Shen, *Phys. Rev. Lett.* **61**, 113 (1988).
 - [4] A. E. Miroshnichenko, E. Brasselet, and Y. S. Kivshar, *Appl. Phys. Lett.* **92**, 253306 (2008); U. A. Laudyn, A. E. Miroshnichenko, W. Krolikowski, D. F. Chen, Y. S. Kivshar, and M. A. Karpierz, *ibid.* **92**, 203304 (2008).
 - [5] B. Ya. Zel'dovich, S. R. Nersisyan, and N. V. Tabiryan, *Sov. Phys. JETP* **61**, 712 (1985).
 - [6] E. Santamato, G. Abbate, P. Maddalena, and Y. R. Shen, *Phys. Rev. A* **36**, 2389 (1987).
 - [7] M. F. Ledney, *JETP Lett.* **85**, 328 (2007).
 - [8] P. G. de Gennes and J. Prost, *The Physics of Liquid Crystals* (Clarendon Press, Oxford, 1993).
 - [9] E. Brasselet, T. V. Galstian, L. J. Dube, D. O. Krimer, and L. Kramer, *J. Opt. Soc. Am. B* **22**, 1671 (2005); D. O. Krimer, Ph.D. thesis, University of Bayreuth, 2004, <http://opus.ub.uni-bayreuth.de/volltexte/2004/98/>.
 - [10] N. V. Tabiryan, A. L. Tabiryan-Murazyan, V. Carbone, G. Ciparrone, C. Umeton, C. Versace, and T. Tschudi, *Opt. Commun.* **154**, 70 (1998).
 - [11] G. Demeter, *Phys. Rev. E* **61**, 6678 (2000); D. O. Krimer, G. Demeter, and L. Kramer, *ibid.* **66**, 031707 (2002).